Sensing and Bio-Sensing Research 29 (2020) 100355

Contents lists available at ScienceDirect

Sensing and Bio-Sensing Research

journal homepage: www.elsevier.com/locate/sbsr

Sandwich SERS immunoassay of human immunoglobulin on silicon wafer compared to traditional SERS substrate, gold film

Zhanar Kunushpayeva, Alisher Rapikov, Aktilek Akhmetova, Alisher Sultangaziyev, Dina Dossym, Rostislav Bukasov*

Chemistry Department, SSH, Nazarbayev University, Nur-Sultan 010000, Kazakhstan

A B S T R A C T

Likely the first application of silicon wafer as a substrate for sandwich immunoassay with Surface Enhanced Raman Scattering (SERS) detection is reported hereafter. Human immunoglobulin (hIgG) was used as a model biomarker in the simultaneous comparative assay on gold film and on Si wafer, an alternative (less expensive and potentially more resistant to surface contamination and non-specific binding) substrate. The Limits of Detection calculated from the data obtained with two-laser wavelength (633 nm and 785 nm) were about 1×10^{-12} mol of antigen or less for both substrates, which is close to the minimal detectable concentration of 30 pM. An approximately logarithmic response was observed across at least a factor of 133 in the dynamic range 0.03–4 nM. However, if four parametric logistic curve is used for the calibration, LOD on silicon would become significantly lower than LOD on gold (3 pM vs 28 pM). A much smaller slope of calibration plot was compensated by a significantly smaller standard deviation in the signal of the blank for the assay on silicon, as compared to the assay on gold. This report may encourage researchers to try silicon or other non-noble metal materials as SERS substrates for the detection of biomarkers.

1. Introduction

The antibodies can detect disease-related markers, and this function is eagerly used in therapeutics [1]. According to the World Health Organization, over 9.6 million deaths in the world were caused by cancer [2], and many of these could be prevented, if early cancer diagnostics were improved by, for instance, a better detection of biomarkers at low concentrations.

Surface Enhanced Raman Scattering (SERS) is a powerful analytical technique that is -known for its high sensitivity and ability to multiplex, due to about one or two order of magnitude more narrow peaks in comparison with peaks of fluorescence or UV–vis spectra. That is why SERS nowadays finds an application in various fields of science. This multifaceted spectroscopy technique gained a special interest in early detection and diagnostics of human diseases such as cancer (e.g. breast cancer [3], and pancreatic cancer [4]), and tuberculosis [5]. The relevant example of SERS-based sandwich immunoassay application in tumor prognosis at early stages is presented by Zhao's research group, who obtained the significantly low limit of detection (LOD) – 0.72 pg/ml – for α-fetoprotein, a biomarker of hepatocellular carcinoma [6]. The detection of interleukin-6, an immune marker with an LOD as low as 2.3 pg/ml, is another good example of SERS implementation in medical diagnostics [7]. The efficiency and outcome of the SERS-based sandwich-type immunoassay can be affected by various conditions such as the ionic strength of buffer solutions, pH, substrate composition, and temperature [8].

Substrate is one of the most important parameters in sandwich-type SERS immunoassays, because it is a foundation for all other components of the assay. Many SERS-based sandwich immunoassays of several scientific groups such as Chang [9], Choo [10], Chung [11], Driskell [12], Krasnoslobotsev [4], Lipert [13], Porter [14], Trau [15] have been conducted on gold films as solid substrates.

Gold and silver film substrates have not only a relatively high cost as a disadvantage, but they may also be susceptible to corrosion, recrystallization and biodegradation [16–18] as well as contamination with mercapto-containing compounds and hydrocarbons, which requires special cleaning/pretreatment [19,20]. However, silicon substrate would not only have significantly lower cost, but it is at least as good as gold as in terms of corrosion (both should be good enough for 16–24 h long assay in PBS). For instance, no significant damage was found on Si mico-photodiode chips immersed for up to 21 months in saline solution, only after 6–12 month in vivo silicon oxide passivation layer of the chip was dissolved [21]. However, after 3 month in vivo corrosion resistance of the titanium pins was found to be superior to that of the gold-plated stainless steel pins, which demonstrated cracks and pores absent in titanium pins [18]. Moreover, silicon is likely to be less prone to contamination than gold film substrate in ambient conditions. Silicon is typically covered with protective and passivating layer of natural silicon oxide [22].

However, as was observed by Whiteside's group while freshly

* Corresponding author.
E-mail address: rostislav.bukasov@nu.edu.kz (R. Bukasov).

https://doi.org/10.1016/j.sbsr.2020.100355
Received 19 March 2020; Received in revised form 24 May 2020; Accepted 26 May 2020

deposited gold substrates are hydrophilic, after exposure to air for several minutes, they become hydrophobic due to the adsorption of adventitious hydrocarbons [23]. That is mainly why, the sandwich SERS immunoassays performed in Porter group on gold substrates has been done on in house made, freshly gold film evaporated substrates [13,24,25].

Recently, the bio-sensing activities of Si wafers as substrates were considered in the fabrication of SERS aptasensor (AgNP@Si) for the detection of ATP [26], Au-coated porous Si for the detection of BSA [27], and AgNP@Si for the detection of 1,3-propanediol [28]. Many of them used silicon substrates, which were still modified with plasmonic components, particularly gold or silver. However, there have been some studies where Si or other semiconductor-based antennas were used without the addition of noble metals, making a promising example of non-plasmonic SERS substrates [29–31]. So far we have not found any reports of Si wafer application as a substrate for SERS sandwich immunoassays, and particularly no reports in which capture molecules/antibodies were attached directly to the silicon wafer substrate.

In this paper, we investigate silicon wafers as a more affordable and potentially more robust substrate than gold film for the SERS sandwich immunoassay of biomarkers. Not only are Si wafers less expensive than smooth gold films (see page 7 of Supplementary Materials), but they would also interact much less with sulfur containing compounds, which are prone to contaminate the gold surface and make the formation of any self-assembled monolayers (SAMs) on gold far less efficient [19].. In many cases, gold film cannot be freshly prepared for its application in the field/clinical analysis, as required in most experiments reported in literature. Gold film is sometimes used months after and far away from when/where it had been deposited. Therefore, it may often be contaminated and demand plasma or piranha solution cleaning before it can be used in the immunoassay. For instance, gold films typically used for immunoassays in the Porter group had either been freshly prepared and used on the same day or plasma cleaned just before they could be used for the assay [14,24], which makes the assay procedure more complicated and costly.

Non-specific binding of proteins creates a major limit to assays' selectivity and sensitivity in the presence of other (not-antigen) proteins [25]. Non-metallic substrates such as Si may not only have a much lower contamination on the surface, but also less non-specific binding (including protein adsorption) on their surface in comparison to gold, which can significantly adsorb S-containing amino acids, abundant in all proteins used in the assay [25,32]. In addition, van der Waals interactions between proteins and silicon would be significantly weaker than the interactions between proteins and gold, as demonstrated by a lower Hamaker constant for Al in comparison to gold [33].

Gold film substrates, used in most sandwich immunoassays, were usually modified with SAM of succinimidyl group containing linkers [34] (e.g. dithiobis(succinimidyl propionate) or DSP). These linkers were supposed to bind a capture antibody to the linker's SAM on gold. However, if modification with linkers was applied, an immunoassay could take more than two days, as described in Driskell et al. publication [35]. However, the redundancy of this procedure was revealed in the publication of Porter's group, where they showed that there was a competition between two processes - aminolysis and hydrolysis - of the DSP-based monolayer [36]. The rate constant, k, for aminolysis, was three orders of magnitude lower than the rate constant for hydrolysis; as a result, the probability of hydrolysis was much greater. Therefore, the linkers should have little if any contribution to antibody binding. An omission of the linker addition step can significantly decrease the time and cost of the sandwich immunoassay, making it more attractive in real life application. Therefore, in the reported assay, capture antibodies would be attached directly to the silicon wafer and gold film, saving assay time and the cost of substrates.

In this paper, Si wafers were tested in a simultaneous sandwich SERS immunoassay with Au film for the detection of human IgG, a classical model biomarker. We also compared Raman measurements obtained with two lasers: 633 and 785 nm, both frequently used in Raman spectroscopy.

2. Materials and methods

2.1. Chemicals and consumables

Commercial microscope slide coated with gold films of 100 nm thickness (99.9% purity), over Cr (thickness = 2–3 nm) layer, were purchased from EFM Co, USA. 60 nm diameter Gold nanoparticles (753653-25 mL) stabilized suspensions in PBS, crystalline Si wafers, human IgG (I4506), anti-human IgG antibody produced from goat (SAB3701279), Bovine Serum Albumin (BSA) A7030–10, Casein blocking buffer, Twin 20 detergent, 4-nitrobenzenethiol (4-NBT) and any other chemicals used in the assay preparation were purchased from Sigma Aldrich. Ultra-pure water was used for all steps of the assay, and it was obtained from Millipore Direct-Q® 3 UV Water Purification System.

2.2. Instrumentation and measurements

Confocal Raman spectrometer (LabRAM Horiba) with 785 nm laser diode and 633 nm Helium-Neon laser, along with a thermoelectrically cooled CCD detector, was used to measure Raman emission intensity in the range 1200–1700 cm^{-1}. The instrument setup: laser power at a sample – approximately 5 mW for 633 nm, and around 10 mW for 785 nm, the objective – ×10, grating - 600 g/mm, map size – 10 × 10 datapoints, step – 200 μm, acquisition time – 2 s, hole – 300 nm, and accumulation – 1.5 maps are collected from each sample before averaging. It is believed that a greater laser spot size results in a lower sampling error, which means it is more reasonable to use the objective ×10 that provides ~25–100 times larger laser spot size than the objective ×50 does [37]. TEM image of 60 nm gold nanoparticle is taken using JEOL JEM-2100 transmission electron microscope.

Smart SPM 1000 Scanning Probe Microscope system from AIST-NT was used to perform AFM measurements. The setting for AFM: cantilever (model – AppNano ACTA-50, material – Si, N-type, 0.01–0.025 Ω/cm, radius of the tip – $r < 10$ nm, k = 37 N/m), rate – 0.8-0.9 Hz, map resolution – 1000 × 1000 pixels, and map sizes were 6 × 6 μm.

2.3. Data processing and calculations

We calculated background corrected Raman intensities (for N—O stretching vibration in 4-NBT molecule) with the peak maximum in the range 1320–1360 cm^{-1} and two peak baseline ranges, 1280–1290 cm^{-1} and 1370–1380 cm^{-1}. To calculate it, we subtracted the average background (BG) (same as the average baseline) from the maximum value of Raman intensity for each spectra, as schematically shown on Fig. 1, in the same way that Raman intensity was calculated in SERS immunoassays by Krasnoslopbodzev group [4,38]. and Bukasov group [39]. All BG corrected spectra were then averaged for each map and for each sample, on each day of measurements. We did measurements of the assay with 633 nm laser excitation in about 2–4 days after the assay was completed. These data are designated as Week A or Week 1 data and they are reported on Fig. S1 and Table S1. We waited about a year until a new 785 nm laser was installed. Then measured those samples with 785 and 633 nm excitation in weeks after about year period of storage: week B, week C. and week D (for 785 nm only). To calculate blank adjusted Raman Intensity for each map, each week and each sample we just subtracted average blank signal (BG-corrected) from the average BG corrected signal for each case. Blank adjusted spectra shown on Figs. 2 and 3 are obtained by subtraction of the blank spectra from the average SERS spectra obtained for each concentration of antibody.

We calculated the LOD as a concentration of analyte at three standard deviations of the blank from the plot of blank adjusted signal vs

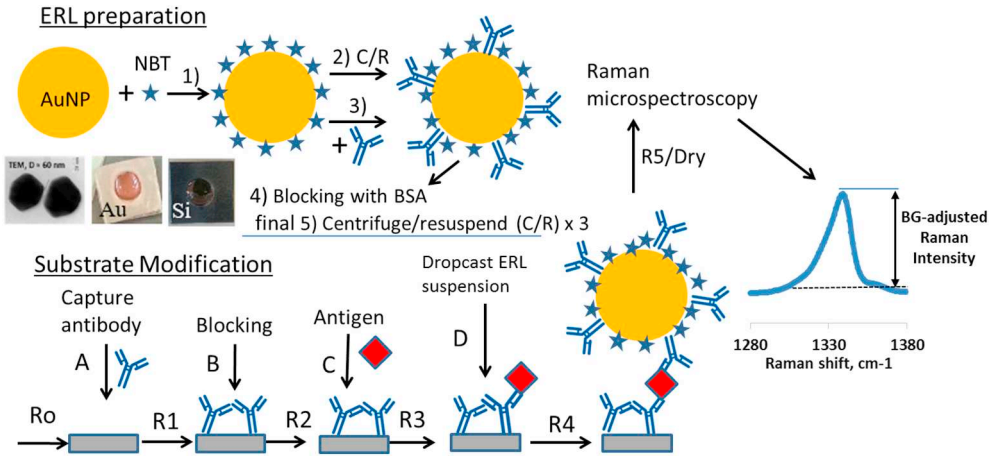

Fig. 1. Scheme of Sandwich SERS immunoassay. Substrates are 100 nm thick gold film evaporated on microscope slide or Silicon wafer. Steps 1) - 5) of ERL preparation are shown above. A,B,C,D steps in substrate modification, where 30 μL of antibody, antigen, casein and ERL suspension, respectively are dropcasted on each address, R/D is rinsing/drying of the substrates, C/R is centrifuge/resuspend in preparation of ERL suspension. Commercially available. 60 nm diameter Au NPs that are used in this paper have a non-ideal spherical shape, which is observed in the TEM image. Pictures of addresses on gold and silicon substrates are shown nearby. (For interpretation of the references to colour in this figure legend, the reader is referred to the web version of this article.)

analyte concentration, according to the formula one shown below.

LOD = 10^ ((3*stdev -b)/a), (1).

Where stdev blank is the standard deviation in the blank signal for 3 different days of measurements, and a and b are the slope and the intercept of the linear calibration plot, respectively.

Since the response of the immunoassay may be S-shaped, we made alternative calculation of LOD using 4 parameter logistic regression analyses: a method commonly used for LOD calculation in bioassays such as ELISA [40]. More details about this method and about the calculation of LOD using logarithmic trend formula (1) are given in Supplementary Information, where the measured values of blank adjusted signals for each concentration, slope, intercept, R^2 and standard deviations of the blank are tabulated for each week of measurements.

The minimum detectable concentration is reported as the lowest measured concentration with a signal above three standard deviations of the blank signal.

The minimum quantifiable concentration is reported as the lowest measured concentration with a signal above ten standard deviations of the blank signal.

2.4. Assay procedure

The general steps of the sandwich immunoassay's procedure are schematically depicted in Fig. 1. Substrates are 100 nm thick gold film evaporated on microscope slide or Silicon wafer, Both microscope slides covered with gold film and Si wafers are cut in squares of

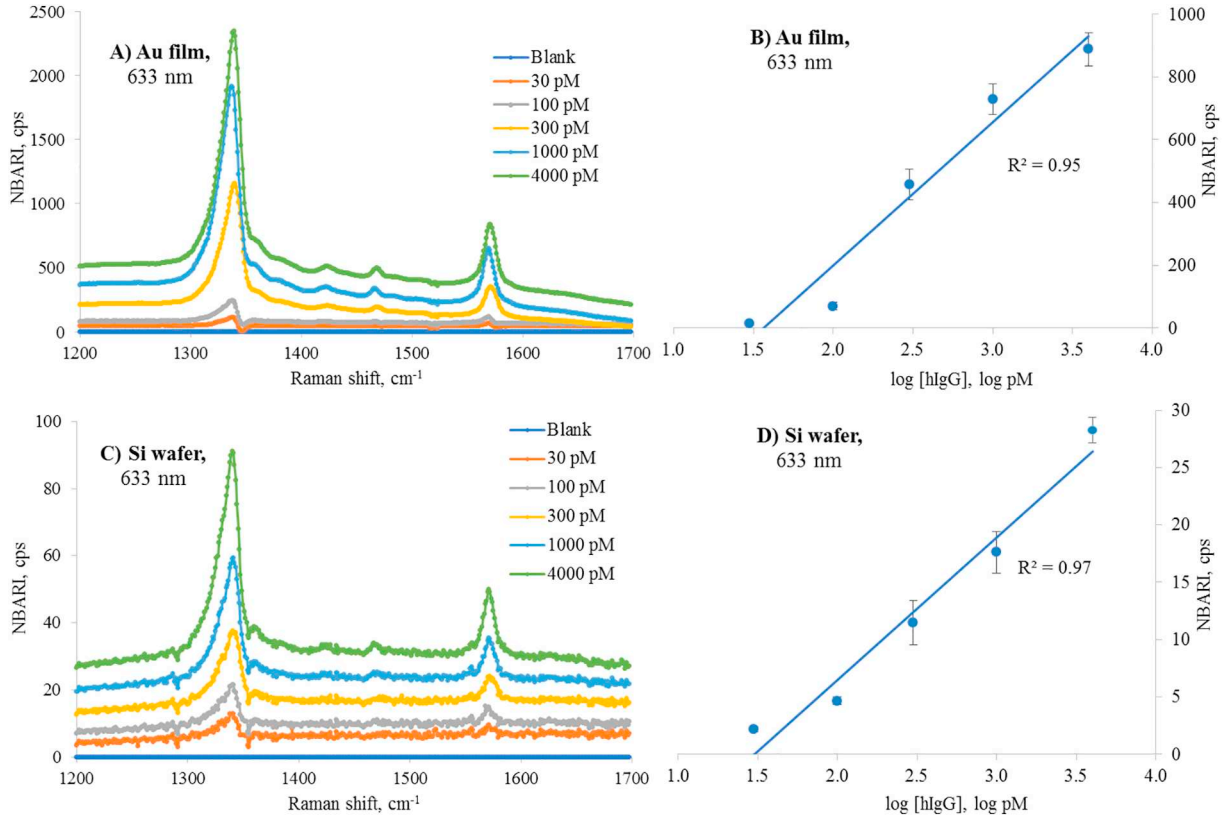

Fig. 2. SERS spectra (A, C) and calibration plots (B, D) for the sandwich immunoassay of hIgG on gold film and Si substrates, obtained with a 633 nm laser. NBARI stands for normalized blank adjusted Raman intensity, which was averaged from 3 different sets of measurements performed on different weeks. (For interpretation of the references to colour in this figure legend, the reader is referred to the web version of this article.)

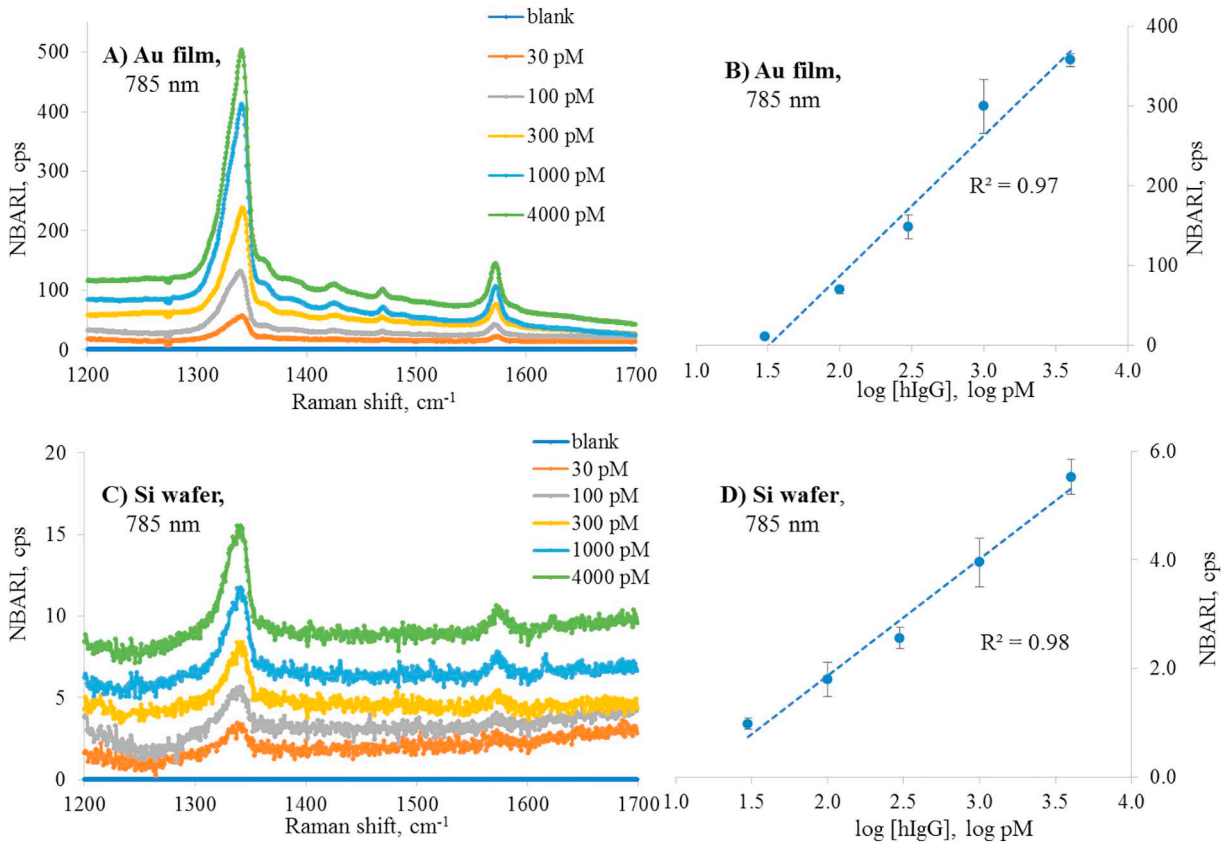

Fig. 3. SERS spectra (A, C) and calibration plots (B, D) for the sandwich immunoassay of hIgG on gold film and Si substrates obtained with a 785 nm laser. NBARI is normalized blank adjusted Raman intensity, which was averaged from 3 sets of measurements performed on different weeks. (For interpretation of the references to colour in this figure legend, the reader is referred to the web version of this article.)

approximately 1.3 × 1.3 cm or 0.5 × 0.5 in. size. Than each of them is covered with parafilm with 5–6 mm diameter hole in the centre, so called address where assay is performed, as described in Supplementary Materials. The purpose of this operation is limit droplet of each solution to the centre of each substrate, since parafilm is hydrophobic. Those 13 × 13 mm substrates are shown on Fig. 1 and labelled Au and Si. From this point, all substrate modification steps in the assay occur in mini-wet chambers, made with inverted Petri dishes. Those Petri dishes tightly cover glass coated with parafilm surface. Multiple water droplets spread among several 1.3 × 1.3 cm size substrates are situated below each Petri dish. The purpose of doing an assay in those mini-wet chambers is to prevent the regent droplet from drying during the assay. During all substrate related steps, a reagent volume of 30 μL was delivered as a droplet on each address The preparation of these addresses is also described in the publication of Gudun et al. [39] Step A, as shown on Fig. 1 of the assay, is the exposure of all addresses to the same solution of capture antibodies (anti-human IgG) for 6 h. They were then rinsed with 2 ml (1 + 1 ml) of PBS buffer (R1), after which each address was blocked for three hours by a Casein Blocking buffer, which is step B on Fig. 1. After another rinsing with the same amount of PBS (R2), Step C involves the exposure of each address to an antigen (human IgG) solution in PBS or a blank (just PBS) for four hours. After rinsing R3, Step D is performed: 30 μl of ERL (extrinsic Raman labels) suspension are dropcasted on each substrate and left in a mini-wet chamber for 8 h. Finally, the substrates were allowed to dry after rinsing, before Raman measurements. The preparation of ERLs is also shown on Fig. 1 schematically: Step 1) 60 nm gold nanoparticles (AuNPs) were modified with Raman reporters (4-NBT) during intense mixing. Then, (step 2)) the AuNPs were then centrifuged and supernatant containing the excess of NBT was discarded. The AuNPs were resuspended in 2 mM borate buffer, capture antibodies (a-hIgG or anti human IgG) were added to the suspension and then tubes with the suspension were stirred for 6 h, which was a step 3). After this, the ERL surface was blocked with BSA solution and they were centrifuged/re-suspended to get rid of unattached antibodies and BSA. Overall, it took less than 24 h to perform the assay. A more detailed procedure of the assay is described on page one of Supplementary Materials.

3. Results and discussion

The normalized blank adjusted Raman spectra and calibration plots for the SERS sandwich immunoassay of human IgG are shown in Figs. 2 and 3 below. Raman measurements were taken using 633 nm He—Ne and 785 nm diode lasers, respectively.

The averaged SERS spectra (A, C) on Figs. 2 and 3 demonstrate a clear trend of the Raman intensity's growth with an increase in the antigen's concentration for both types of SERS-active substrates. The signals of analyte are approximately one order of magnitude greater on the gold substrate than on the silicon substrate. Fig. 2 and Fig. 3 demonstrate, the overall trend for 5 data points (30 to 4000 pM), which for two substrates and for both lasers (633 nm and 785 nm) may be approximated as linear logarithmic trend with R^2 values a bit higher on Si (0.97 and 0.98) than R^2 values on gold (0.95 and 0.97), when we use data averages from all 3 various weeks of measurements. However, since the calibration trend for SERS assay of a biomarker can be similar to one obtained from ELISA assays, it can be represented as a curve, approximated with 4-parameter logistic regression analysis [41]. Therefore we made calculations of LODs using two methods: 1-st ("conservative") from the linear segment of calibration plot (10, 100, 300, 1000, 4000 pM) and the 4-th using four parameter logistic model as shown in details in Tables S1, S2 and Figs. S1 and S2 of Supplementary Materials When we apply "conservative" linear logarithmic

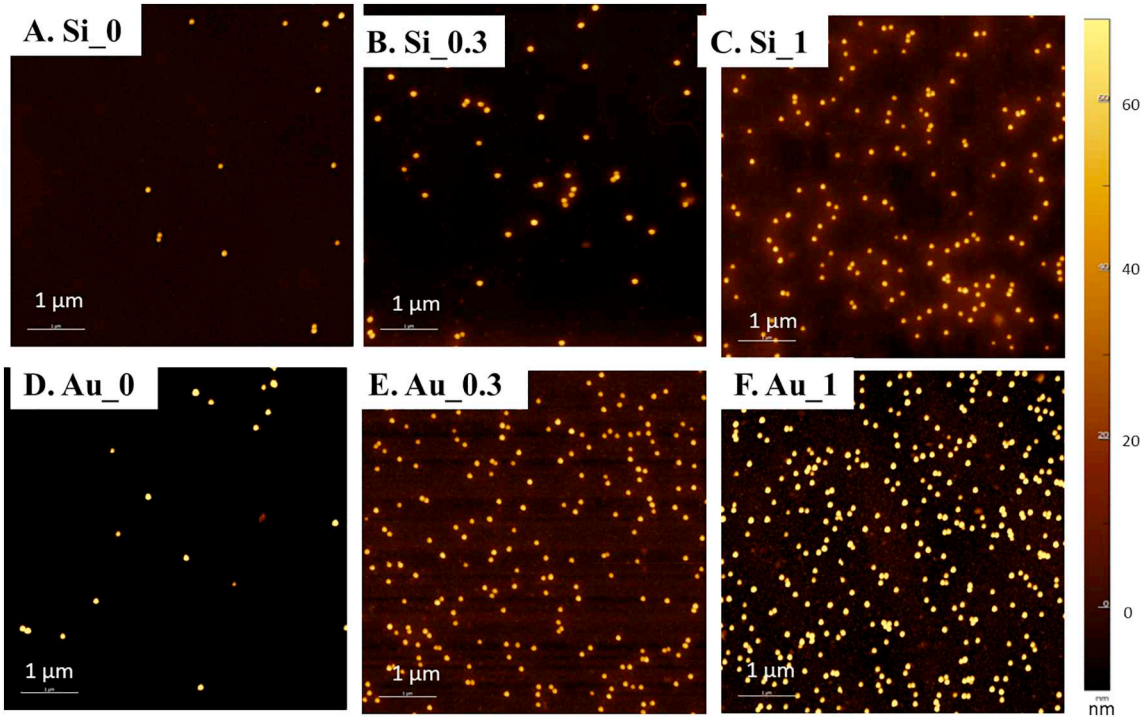

Fig. 4. Representative AFM maps of increasing hIgG concentration: 0 (blank), 0.3 nM, 1 nM for A, B, C – Si, and D, E, F – gold film substrates. (For interpretation of the references to colour in this figure legend, the reader is referred to the web version of this article.)

calibration, the signal and the slope is typically decreasing from the first set of measurements (week A) to the following set of measurements (week B and week C) and LODs in most cases are increasing. This trend is predictable since the samples cannot have indefinite stability due to eventual thiol desorption and possible partial sample bleaching with laser light upon measurements. In fact it may be surprising that even with one year time lapse between week A and following (weeks B and C) measurements with 633 nm laser the calibration trend remain more or less intact, which indicates a fairly good stability of the samples and capacity for multiple re-measurements after a few month of time. This feature of the method might be used as advantage in detection of so called doping or prohibited substances in sport or in forensic analysis. However, the measurements within just one week after assay completion produced the best results. As shown in Table S1 in Supplementary Materials for 633 nm laser excitation for both assays on gold and on silicon LOD after first measurements got a bit worse. It increased from 34 to 39, 40 pM for assay on gold and it increased from 25 to 38, 37 pM for assay on silicon. The linearity R^2 for calibration plots decreased as samples were re-measured from 0.97 to 0.93–0.95 for both assays on gold and silicon.

LOD values for assays on gold and silicon calculated by the same approach are more or less similar. For instance for week one (the most freshly obtained data), when 633 nm laser data and "conservative" linear logarithmic 5 data point calibration were used, LOD on gold is 34 pM and LOD on silicon is 25 pM. The LODs for the same kind of calibration made from 785 nm laser are 33 pM on gold and 28 pM on silicon, but logarithmic trend R^2 on gold was not nearly as good as R^2 on silicon (0.96 and 0.98, respectively). Overall there are no significant differences between two lasers (633 and 785 nm) in terms of LODs calculated for assays on both substrates. However, the y-scale (SERS signal) and slope on calibration plots decreased about several-fold for both gold and silicon, when we switch from 633 nm laser excitation to 785 nm laser excitation. That is expected, since LSPR resonance of gold nanoparticles (λ max in suspension ~540 nm) on both gold film and silicon should be closer to 633 nm rather than 785 nm excitation wavelength. Still for any practical applications, 785 nm lasers can be used about as well as 633 nm laser for the measurements of sandwich SERS immunoassays on both substrates gold film and silicon.

While the slope of signal vs log [hIgG] on the calibration plot for gold, is much higher than the same kind of slope for the assay on silicon, which would increase the LOD according to Formula 1, there is a strong opposite effect from a much lower standard deviation of the blank on silicon relative to the standard deviation of the blank on gold (e. g 0.22 cps vs 3.01 cps respectively for week A, 633 nm measurements). In fact even relative standard deviations for signal on silicon are roughly two times lower than corresponding relative standard deviations for signal on gold. For instance average for 2 lasers RSDs, % for concentration of 30pM of hIgG are 12.1% on gold and 5.5% on silicon.

However when we use four parameter logistic model for calibration and LOD calculation as illustrated on Fig. S2 of Supplementary Materials, the LOD for silicon are significantly lower than LOD for gold: 3 pM and 28 pM respectively.

The silicon substrates performed at least as well as gold substrates in terms of the lowest detectable concentration for this type of SERS sandwich immunoassay (for measurements with both lasers (633 and 785 nm)).

The representative AFM maps taken for blank (0), 300 and 1000 pM hIgG samples for both substrates are shown on Fig. 4. There is an evident increase in the number of nanoparticles per area with an increase in antigen concentration for both substrates. Table S3 in Supplementary Materials contains numerical data obtained from 36 AFM maps from six samples, in which 5060 nanoparticles (ERLs) were counted. The Number ERL/Area (per 1 μm^2) increases from 0.55 to 6.5 to 10.1 ERL/μm^2 on gold. On silicon, it increases from 0.38 to 1.6 to 4.5 ERL/ μm^2. Overall, the correlation between the surface concentration of ERLs (ERLs/μm^2) calculated from AFM maps and the measured background adjusted Raman Intensity is quite high, with an average (of 633 and 785 nm excitation) R^2 equal to 0.98.

We also calculated the ratio of Raman intensity to Number ERL/Area (ERLs/μm^2) for all six samples for both lasers and demonstrated it in a bar graph on Fig. 5. All numbers behind this bar graph, including those needed to calculate error bars, are included in Table S3 in

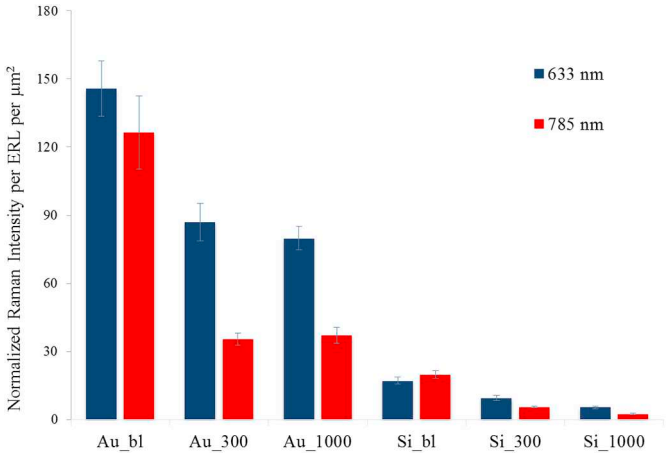

Fig. 5. Normalized Raman intensity per (ERL per Area, μm^2) for 633 nm and 785 nm lasers on Si and gold film substrates at various concentrations of human IgG from blank to 300 pM and 1000pM. (For interpretation of the references to colour in this figure legend, the reader is referred to the web version of this article.)

Supplementary Materials. Fig. 5 shows that the Raman signal per nanoparticle is clearly higher on gold than on silicon, by about one order of magnitude. In fact, from Table S3, we can calculate that on average, the ratio of Raman signal per ERL on gold to this parameter on silicon, for the same antigen concentration, is about 11 for 633 nm excitation and about 9 for 785 nm excitation. This observation is in general agreement with the ratio of SERS enhancement factor (EF) on gold to the EF on silicon, calculated from a combination of Raman and AFM maps in the publication of Sergiienko at al [42]. However, Fig. 5 also shows some decrease in Raman signal per nanoparticle as the concentration of antigen increases, particularly between a blank and 0.3 nM concentration of human IgG. Fractions of single nanoparticles among all the nanoparticles counted in the assay did not change very much from sample to sample on both substrates, remaining within 70 to 80%. In fact, the average fraction of single ERLs was quite similar for silicon and for gold: 77% and 76% of ERLs were singles, on silicon and gold film respectively. Therefore, we may hypothesize that another factor is responsible for this decrease in signal per ERL, or an equivalent decrease in the enhancement factor when an antigen becomes present (no antigen in the blank) and when the surface concentration of ERLs increases. For instance, ERL-substrate distance is likely to increase on average when an antigen is present, and plasmonic coupling between the gold nanoparticle and substrate may weaken, decreasing the SERS EF for 4-NBT on the nanoparticle surface. Upon an increase in surface concentration of nanoparticles, the extinction cross-section of each nanoparticle and the SERS EF would both slightly decrease. Moreover, these effects are not very large (well within a factor of 2 for 633 nm laser and a factor of 3 for 785 nm laser). They are present in assays on both gold and silicon substrates; the most important consideration is that they do not significantly spoil the assay performance, at least for the 133 range of analyte concentrations.

Eventually, we are planning to test other non-noble metal materials as affordable substrates in sandwich SERS immunoassays, as well as probe selectivity of human IgG detection vs signal from non-specific binding of other proteins, on both silicon and gold film substrates.

4. Conclusions

Finally, we can summarize that the LOD of a biomarker in a sandwich SERS immunoassay on Si wafer by the most conservative estimate is comparable or even lower than the LOD in the same assay on Au film. The conservative logarithmic calculation shows LODs for both substrates about 0.03 nM, or about 1×10^{-12} mol of analyte. However, if calibration is made with four parameter logistic model assay on Si substrates outperforms assays on gold almost by an order of magnitude (LODs of 3 pM on Si and 28 pM on gold respectively). The assays of hIgG on both substrates show the same minimum detectable (30 pM) and minimum quantifiable concentrations (100 pM) at 633 nm excitation. Overall, an SERS signal of one magnitude less per gold nanoparticle for Silicon and a much lower slope on the calibration plot is compensated by the same order of decrease in the standard deviation of the Raman signal. In fact even relative standard deviation for measurements on silicon is lower than relative standard deviation for measurements on gold. The assay preparation was completed in less than 24-h; it did not require relatively expansive linker molecules since the assay applied direct adsorption of a capture antibody to both substrates. The stability of the nanoparticle – substrate system SERS response - was relatively high and therefore, the assay results could be re-measured a few weeks after the original measurements. Since both lasers, 633 and 785 nm, delivered about the same LOD and minimum detectable concentrations, as well as a similar dynamic range for silicon as a substrate, we may assume that the assay on Si can also work in a relatively broad range of excitation wavelength. Good correlation between the Raman signal and the number of particles per area obtained from the AFM supports these observations. Overall, silicon can compete and even outcompete with gold not only with 633 nm laser but with 785 nm laser. Therefore, we think that silicon should receive more attention as a relatively cost effective and inert/robust substrate for SERS sandwich immunoassays or other SERS applications related to bio sensing (where non-specific binding to a substrate may pose an obstacle). In some applications, it may become the SERS substrate of choice, advancing the practical applicability of SERS based analytical methods.

Data availability

The data used to support the findings of this study are included within the article and the supplementary information file.

Declaration of Competing Interests

The authors declare that there is no conflict of interest regarding the publication of this paper.

Funding statement

This research is supported by the Nazarbayev University Faculty Development Competitive Research grant 090118FD5352 (Kazakhstan) “Fundamental and applied SERS for detection of cancer biomarkers” (FASERSDCB)

Author contribution statement

Zhanar Kunushpayeva, Alisher Rapikov, Aktilek Akhmetova, Alisher Sultangaziyev, Dina Dossym are involved into substrate preparation, assay performance, Raman and AFM meassurements, data processing and preparation of figures. Aktilek Akhmetova and Alisher Sultangaziyev also contributed to literature review and writing the first draft of introduction. Bukasov Rostislav is responsible for visualization, funding, supervision of experiments, data processing, preparation of figures, writing the final version of the manuscript .

Appendix A. Supplementary data

Supplementary data to this article can be found online at https://doi.org/10.1016/j.sbsr.2020.100355.

References

[1] M. Suzuki, C. Kato, A. Kato, Therapeutic antibodies: their mechanisms of action and the pathological findings they induce in toxicity studies, J. Toxicol. Pathol. 28 (3) (2015) 133–139.

[2] Organization, W. H. Cancer, https://www.who.int/news-room/fact-sheets/detail/cancer.

[3] S. Cervo, E. Mansutti, G. Del Mistro, R. Spizzo, A. Colombatti, A. Steffan, V. Sergo, A. Bonifacio, SERS analysis of serum for detection of early and locally advanced breast cancer, Anal. Bioanal. Chem. 407 (24) (2015) 7503–7509.

[4] A.V. Krasnoslobodtsev, M.P. Torres, S. Kaur, I.V. Vlassiouk, R.J. Lipert, M. Jain, S.K. Batra, Y.L. Lyubchenko, Nano-immunoassay with improved performance for detection of cancer biomarkers, Nanomedicine 11 (1) (2015) 167–173.

[5] A.C. Crawford, L.B. Laurentius, T.S. Mulvihill, J.H. Granger, J.S. Spencer, D. Chatterjee, K.E. Hanson, M.D. Porter, Detection of the tuberculosis antigenic marker mannose-capped lipoarabinomannan in pretreated serum by surface-enhanced Raman scattering, Analyst 142 (1) (2017) 186–196.

[6] J. Zhao, C. Wu, L. Zhai, X. Shi, X. Li, G. Weng, J. Zhu, J. Li, J.-W. Zhao, A SERS-based immunoassay for the detection of α-fetoprotein using AuNS@ag@SiO2 core-shell nanostars, J. Mater. Chem. C 7 (27) (2019) 8432–8441.

[7] A. Kaminska, K. Winkler, A. Kowalska, E. Witkowska, T. Szymborski, A. Janeczek, J. Waluk, SERS-based immunoassay in a microfluidic system for the multiplexed recognition of interleukins from blood plasma: towards Picogram detection, Sci. Rep. 7 (1) (2017) 1–11.

[8] R. Reverberi, L. Reverberi, Factors affecting the antigen-antibody reaction, Blood Transfus. 5 (4) (2007) 227–240.

[9] C.-C. Lin, Y.-M. Yang, Y.-F. Chen, T.-S. Yang, H.-C. Chang, A new protein a assay based on Raman reporter labeled immunogold nanoparticles, Biosens. Bioelectron. 24 (2) (2008) 178–183.

[10] M. Lee, K. Lee, K.H. Kim, K.W. Oh, J. Choo, SERS-based immunoassay using a gold array-embedded gradient microfluidic chip, Lab Chip 12 (19) (2012) 3720–3727.

[11] K. Shin, J.-H. Cho, M.-Y. Yoon, H. Chung, Use of multiple peptide-based SERS probes binding to different epitopes on a protein biomarker to improve detection sensitivity, Anal. Chem. 88 (7) (2016) 3465–3470.

[12] M.A. Penn, D.M. Drake, J.D. Driskell, Accelerated surface-enhanced Raman spectroscopy (SERS)-based immunoassay on a gold-plated membrane, Anal. Chem. 85 (18) (2013) 8609–8617.

[13] G. Wang, R.J. Lipert, M. Jain, S. Kaur, S. Chakraboty, M.P. Torres, S.K. Batra, R.E. Brand, M.D. Porter, Detection of the potential pancreatic cancer marker MUC4 in serum using surface-enhanced Raman scattering, Anal. Chem. 83 (7) (2011) 2554–2561.

[14] M.D. Porter, R.J. Lipert, L.M. Siperko, G. Wang, R. Narayanan, SERS as a bioassay platform: fundamentals, design, and applications, Chem. Soc. Rev. 37 (5) (2008) 1001–1011.

[15] Y. Wang, S. Rauf, Y.S. Grewal, L.J. Spadafora, M.J.A. Shiddiky, G.A. Cangelosi, S. Schlücker, M. Trau, Duplex microfluidic SERS detection of pathogen antigens with Nanoyeast single-chain variable fragments, Anal. Chem. 86 (19) (2014) 9930–9938.

[16] H. Kosslick, H. Sauer, T. Just, U. Vick, G. Fulda, L. Jonas, Biodegradation of gold and platinum implants in rats studied by electron microscopy more information, International Journal of Physics Research and Applications 2 (2019).

[17] Z. Lu, H. Si, Z. Li, J. Yu, Y. Liu, D. Feng, C. Zhang, W. Yang, B. Man, S. Jiang, Sensitive, reproducible, and stable 3D plasmonic hybrids with bilayer WS2 as nanospacer for SERS analysis, Opt. Express 26 (17) (2018) 21626–21641.

[18] G. Palaghias, G. Eliades, G. Vougiouklakis, In vivo corrosion behavior of gold-plated versus titanium dental retention pins, J. Prosthet. Dent. 67 (2) (1992) 194–198.

[19] T. Ishida, S. Tsuneda, N. Nishida, M. Hara, H. Sasabe, W. Knoll, Surface-conditioning effect of gold substrates on Octadecanethiol self-assembled monolayer growth, Langmuir 13 (17) (1997) 4638–4643.

[20] C.G. Worley, R.W. Linton, Removing sulfur from gold using ultraviolet/ozone cleaning, J. Vac. Sci. Technol. A 13 (4) (1995) 2281–2284.

[21] H. Hämmerle, K. Kobuch, K. Kohler, W. Nisch, H. Sachs, M. Stelzle, Biostability of micro-photodiode arrays for subretinal implantation, Biomaterials 23 (3) (2002) 797–804.

[22] R.V. Ghiţă, C. Logofatu, C. Negrila, F. Ungureanu, C. Cotîrlan, A. Manea, M. Lazarescu, C. Ghica, Study of SiO2/Si Interface by Surface Techniques, (2011).

[23] C.D. Bain, E.B. Troughton, Y.T. Tao, J. Evall, G.M. Whitesides, R.G. Nuzzo, Formation of monolayer films by the spontaneous assembly of organic thiols from solution onto gold, J. Am. Chem. Soc. 111 (1) (1989) 321–335.

[24] J.H. Granger, M.C. Granger, M.A. Firpo, S.J. Mulvihill, M.D. Porter, Toward development of a surface-enhanced Raman scattering (SERS)-based cancer diagnostic immunoassay panel, Analyst 138 (2) (2013) 410–416.

[25] G. Wang, H.-Y. Park, R.J. Lipert, M.D. Porter, Mixed Monolayers on gold nanoparticle labels for multiplexed surface-enhanced raman scattering based immunoassays, Anal. Chem. (Washington, DC, U. S.) 81 (23) (2009) 9643–9650.

[26] H. Shi, N. Chen, Y. Su, H. Wang, Y. He, Reusable Silicon-Based Surface-Enhanced Raman Scattering Ratiometric Aptasensor with High Sensitivity, Specificity, and Reproducibility, Anal. Chem. (Washington, DC, U. S.) *89* (19) (**2017**) 10279–10285.

[27] V. Kalimuthu, S. Rath, One-step synthesis of au-coated porous silicon as a surface enhanced Raman scattering substrate for biomolecule detection, Mater. Lett. 204 (2017) 115–119.

[28] W.C. Zhao, H.R. Ren, X. Zhang, Z. Wang, Y.M. Zhao, L. Liu, Z.L. Wu, H.J. Xu, Rapid determination of 1,3-propanediol in fermentation process based on a novel surface-enhanced Raman scattering biosensor, Spectrochim. Acta, Part A 211 (2019) 227–233.

[29] I. Alessandri, E. Biavardi, A. Gianoncelli, P. Bergese, E. Dalcanale, Cavitands endow all-dielectric beads with selectivity for Plasmon-free enhanced Raman detection of Nε-methylated lysine, ACS Appl. Mater. Interfaces 8 (24) (2016) 14944–14951.

[30] G. Magno, B. Belier, G. Barbillon, Al/Si nanopillars as very sensitive SERS substrates, Materials 11 (9) (2018) 1534/1–1534/9.

[31] M. Caldarola, P. Albella, E. Cortés, M. Rahmani, T. Roschuk, G. Grinblat, R.F. Oulton, A.V. Bragas, S.A. Maier, Non-plasmonic nanoantennas for surface enhanced spectroscopies with ultra-low heat conversion, Nat. Commun. 6 (1) (2015) 7915.

[32] S. Choi, J. Chae, Methods of reducing non-specific adsorption in microfluidic biosensors, J. Micromech. Microeng. 20 (7) (2010) 075015/1–075015/9.

[33] G.L. Klimchitskaya, U. Mohideen, V.M. Mostepanenko, Casimir and van der Waals forces between two plates or a sphere (lens) above a plate made of real metals, Physical Review A - Atomic, Molecular, and Optical Physics 61 (6) (2000) 1–12.

[34] H.Y. Park, J.D. Driskell, K.M. Kwarta, R.J. Lipert, M.D. Porter, C. Schoen, J.D. Neill, J.F. Ridpath, Ultrasensitive immunoassays basedon surface-enhanced Raman scatteringby immunogold labels, 103 (2006), pp. 427–446.

[35] J.D. Driskell, K.M. Kwarta, R.J. Lipert, M.D. Porter, J.D. Neill, J.F. Ridpath, Low-level detection of viral pathogens by a surface-enhanced Raman scattering based immunoassay, Anal. Chem. 77 (19) (2005) 6147–6154.

[36] C.Y. Lim, N.A. Owens, R.D. Wampler, Y. Ying, J.H. Granger, M.D. Porter, M. Takahashi, K. Shimazu, Succinimidyl ester surface chemistry: implications of the competition between aminolysis and hydrolysis on covalent protein immobilization, Langmuir 30 (43) (2014) 12868–12878.

[37] A.C. Crawford, A. Skuratovsky, M.D. Porter, Sampling error: impact on the quantitative analysis of nanoparticle-based surface-enhanced Raman scattering immunoassays, Anal. Chem. 88 (12) (2016) 6515–6522.

[38] R. Bukasov, T.A. Ali, P. Nordlander, J.S. Shumaker-Parry, Probing the plasmonic near-field of gold nanocrescent antennas, ACS Nano 4 (11) (2010) 6639–6650.

[39] K. Gudun, Z. Elemessova, L. Khamkhash, E. Ralchenko, R. Bukasov, Commercial gold nanoparticles on untreated Aluminum foil: versatile, sensitive, and cost-effective SERS substrate, J. Nanomater. 2017 (2017) 8.

[40] C.A. Holstein, M. Griffin, J. Hong, P.D. Sampson, Statistical method for determining and comparing limits of detection of bioassays, Anal. Chem. 87 (19) (2015) 9795–9801.

[41] M.A. Oconnell, B.A. Belanger, P.D. Haaland, Calibration and assay development using the 4-parameter logistic model, Chemom. Intell. Lab. Syst. 20 (2) (1993) 97–114.

[42] S. Sergiienko, K. Moor, K. Gudun, Z. Yelemessova, R. Bukasov, Nanoparticle-nanoparticle vs. nanoparticle-substrate hot spot contributions to the SERS signal: studying Raman labelled monomers, dimers and trimers, Phys. Chem. Chem. Phys. 19 (6) (2017) 4478–4487.